



ELSEVIER

Contents lists available at ScienceDirect

Mechanical Systems and Signal Processing

journal homepage: www.elsevier.com/locate/ymssp

Non-reciprocity in nonlinear chirality-induced autoparametric periodic structures

Tianjun Yu^a, Yong Cheng^a, Sha Zhou^{b,*}^a Key Laboratory of Dynamics and Control of Flight Vehicle, Ministry of Education and School of Aerospace Engineering, Beijing Institute of Technology, Beijing 100081, China^b Department of Engineering Mechanics, Zhejiang University, Hangzhou 310027, China

ARTICLE INFO

Keywords:

Metamaterial
Chiral microstructure
Geometric nonlinearity
Autoparametric modulation
Non-reciprocity
Band topology

ABSTRACT

Periodic structure with spatiotemporally modulated properties has become a rising concern due to its unusual behavior to manipulate non-reciprocal wave propagation. In this paper, by taking advantage of the asymmetric architecture of nonlinear chiral microstructures, we propose a novel autoparametric modulated periodic structure and investigate its global dynamics, non-reciprocal and topological effect. An analytical formulation for deriving the evolution equations and solving the dispersion relations of the autoparametric system is presented by combining the multiple-time scales perturbation method and Floquet-Bloch theorem. Non-reciprocal wave behavior and band topology of the autoparametric modulated periodic structure are analyzed and demonstrated by numerical calculations. We envision that the autoparametric modulated configuration realized by nonlinear chirality may serve as a building block for realizing one-way propagation and mechanical logic gate in passive or active ways.

1. Introduction

Reciprocity is a fundamental physical principle stating that wave propagation relating two points is independent of the choice of source and receiver [1,2]. Breaking reciprocity enables the realization of one-way wave propagation, expecting to bring numerous potential applications to wave communication, vibration isolation and energy harvesting. Non-reciprocal wave propagation can be achieved by resorting to the chiral inertial coupling in gyroscopic phononic crystals [3,4], or by the combination of structural asymmetry and high order harmonic generation induced by nonlinearity [5–11]. Recently, harnessing the spatiotemporal modulation over material properties to break reciprocity have received considerable attentions [12–20], and experimental demonstrations of the non-reciprocity in dynamic one-dimensional phononic crystals and metamaterials have been reported [21,22]. Time-modulated properties of structural materials are tailored in active ways primarily through the coupling of multiple physical fields at the microstructure level. Purely mechanical small-on-large coupling based on the nonlinear mechanism can be also utilized to design phononic lattices with the non-reciprocity [23,24]. On the other hand, the time modulation of constitutive properties is greatly valued for it offers a necessary degree of freedom (DOF) for realizing the non-trivial band topology in mechanical systems via breaking time-reversal symmetry. Mechanical topological insulators can guarantee the robustness of one-way topological edge modes and stay immune to backscattering by defects, damping dissipation, sharp corners, and modulation disorders [12,25,26].

Autoparametric structural systems are vibrating systems consisting of at least a primary subsystem and secondary one which are

* Corresponding author.

E-mail address: lilyzhou191@hotmail.com (S. Zhou).

nonlinearly coupled [27]. The effects of the primary system on the secondary system are interpreted by parametric excitation terms included in the equations of motion of the autoparametric systems [28]. The autoparametric phenomena are frequently encountered in engineering. For instance, the pitch motion and the rolling motion for a vessel in a longitudinal sea couple to each other via nonlinear buoyancy. The engines of airplanes mounted under the wings by elastic suspenders is another typical example in which the vertical motion of the wing and the swinging motion of the suspended engines form an autoparametric system.

In this paper, we propose a novel scheme to create the time-modulated properties by integrating the metamaterial design with the concept of autoparametric system. Metamaterials are artificial materials that derive unusual dynamic properties mainly from the constitutive microstructures [29–33]. In the present study, artificial metamaterials are constituted by autoparametric unit cells, and the temporally modulated dynamics stems from autoparametric mode coupling.

The paper is organized as follows: In Section 2, by introducing nonlinear chiral rotational DOF into mechanical Drude-type model, we propose a novel autoparametric modulated periodic structure. To characterize the global dynamics and intrinsic non-reciprocity of such autoparametric modulated system, a procedure to derive the evolution equations and calculate the dispersion relations based on the multiple-time scales perturbation method and Floquet-Bloch theorem is presented in Section 3. In Section 4, numerical simulations are performed to validate the analytical results. One-way wave propagation and frequency conversion due to the autoparametric modulation are illustrated. The non-trivial topological characterization of wave dispersion and the bulk-edge correspondence relationship are also examined for the quasi-static scenario. In Section 5, we end this paper with concluding remarks.

2. Geometric model of autoparametric periodic structure

Differing from the mechanical systems based on parametric resonances [34], the essential feature of an autoparametric system is that it should consist of at least a primary system and a secondary system that are coupled. Such system is expected to exhibit its wave control capability by means of *one degree of freedom to manipulate the other*. The proposed one-dimensional mass-spring model of autoparametric periodic structure with lattice distance a is shown in Fig. 1. Four linear elastic springs are pin-connected to an oscillator of mass m and a rigid disk of radius R and rotational inertia J . The included angles between two inclined springs with stiffness G and horizontal springs with stiffness K are both θ in an initial undeformed configuration. Here, chiral rotational vibration of disks is introduced as a primary DOF to manipulate the longitudinal DOF of oscillators at the unit cell scale. The chiral geometry is suggested since the quadratic nonlinear terms necessary for the autoparametric coupling automatically arise in the finite deformation regime, as addressed further below. The inclined springs of rest length $R/\tan\theta$ satisfy linear force–displacement relationship $f_r = G\delta$. The length changes of the left and right springs in large deformation can be expressed as $\delta_l = R\epsilon p + \left\{ \sqrt{(R/\sin\theta - \epsilon u)^2 - R^2} - [\arccos(R/(R/\sin\theta - \epsilon u)) - \pi/2 + \theta]R - R/\tan\theta \right\}$, $\delta_r = R\epsilon p - \left\{ R/\tan\theta - [\pi/2 - \theta - \arccos(R/(R/\sin\theta + \epsilon u))]R + \sqrt{(R/\sin\theta + \epsilon u)^2 - R^2} \right\}$, respectively. Herein, ϵ is a small, dimensionless parameter to mark the orders of the amplitude p of the rotational vibration and the amplitude u of the longitudinal wave. The linear force–displacement relationship of horizontal springs reads $f_t = Kq$. According to the dynamic equilibrium condition, the equations of motion for the j th cell can be expressed by retaining nonlinear terms up to $O(\epsilon^2)$ as

$$m \frac{d^2 u_j}{dt^2} - k(u_{j-1} - 2u_j + u_{j+1}) + (2K + 2G\cos^2\theta)u_j + 2G\tan\theta\sin^2\theta p_j u_j = 0$$

$$J \frac{d^2 p_j}{dt^2} + 2R^2 G p_j + G\tan\theta\sin^2\theta u_j^2 = 0$$

Introducing the dimensionless variables and parameters

$$\bar{u}_{j-1} = \frac{u_{j-1}}{a}, \bar{u}_j = \frac{u_j}{a}, \bar{u}_{j+1} = \frac{u_{j+1}}{a}, \tau = \omega_0 t = \sqrt{\frac{k}{m}}t,$$

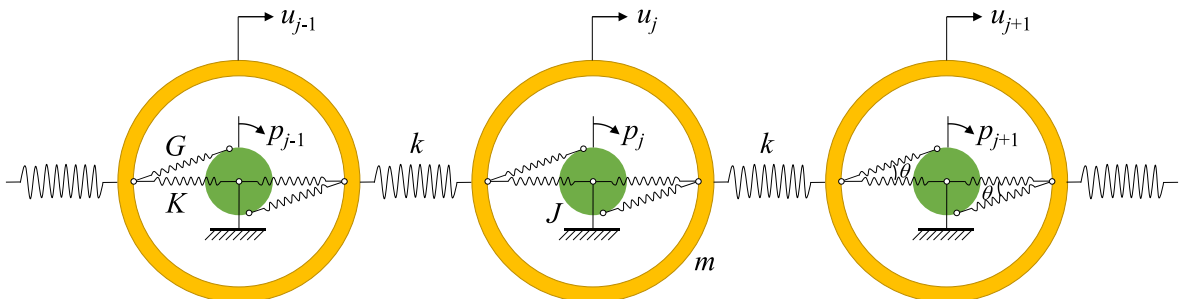


Fig. 1. The 1D representative mass-spring model attached with chiral oscillators.

$$\alpha = \frac{G}{k}, \beta = \frac{K}{k}, \gamma = \frac{R}{a}, \mu = \frac{J}{mR^2} \tag{2}$$

Under this rescaling, Eq. (1) become, after dropping all overbars for convenience

$$\begin{aligned} \ddot{u}_j - (u_{j-1} - 2u_j + u_{j+1}) + 2(\beta + \alpha \cos^2 \theta)u_j + 2\alpha \tan \theta \sin^2 \theta p_j u_j &= 0 \\ \ddot{p}_j + \frac{2\alpha}{\mu} p_j + \frac{\alpha \tan \theta \sin^2 \theta}{\mu \gamma^2} u_j^2 &= 0 \end{aligned} \tag{3}$$

where the overdot denotes differentiation with respect to τ .

According to the equations of motion in a unit cell, the chiral rotational vibration p is decoupled with the longitudinal wave u when deformations are infinitesimal, but coupled when geometric nonlinearity is considered. To be specific, the rotational vibration acts on the longitudinal wave as a parametric excitation via the quadratic nonlinearity with cross-product term. Conversely, the longitudinal wave transports dynamical responses into the rotational vibration via the quadratic nonlinearity with self-product term, resulting in the generation of even harmonics of the rotational vibration. Such autoparametric system is two-way coupled when the amplitude of the rotational vibration and the amplitude of the longitudinal wave are in the same order of magnitude. When the amplitude of the rotational vibration is significantly larger than that of the longitudinal wave, the feedback of longitudinal wave to rotational vibration can be ignored. In other words, one-way coupling with the small-on-large modulation would be created naturally. As we will discuss in the following sections, in a super cell, the rotational vibration with traveling phases acting on the longitudinal wave can be degenerated to, in the sense of perturbation, a wave-like spatiotemporal modulation of the stiffness properties. The presented autoparametric system, in fact, as a macro system, contains the small-on-large modulation system and incorporates the active excitation of conventional spatiotemporal modulation system as a part of the macro system itself. Thus, the conservative autoparametric system (3) supplies an effective solution for exploring purely mechanical spatiotemporal modulation in passive ways when mechanical damping is neglected. When the mechanical damping is small but cannot be ignored, it is predicted that such autoparametric system can be applied to a limited time operation scenario in order to generate non-reciprocal wave propagation. On the other hand, if the rotational vibration is excited forcedly by using active components, the longitudinal wave will then be parametrically excited through the direct coupling of mechanical force. Thereby, a new type of spatiotemporal modulation system in active ways will be expected. Based on this kind of autoparametric dynamical system, we are inspired to construct modulated periodic structures with quadratic nonlinearity by taking advantage of the asymmetric property of chiral structures.

In the following sections, by releasing the chiral rotational DOF in a super cell, based on the conservative autoparametric dynamical system (4), we design a wave-like modulated periodic structure and study the wave non-reciprocity in different cases of fast autoparametric modulation, moderate autoparametric modulation and quasi-static modulation, respectively. Hereafter, the modulation speed will be classified according to the vibration frequency of the rotational DOF.

3. Multiple-time scales perturbation method for dispersion analysis

To assemble a traveling wave modulation, at least three sub-cells distributed in real space with specific phases are required. Without loss of generality, we consider the autoparametric modulated super cell structure composed of three sub-cells, as shown in Fig. 2. By applying the Floquet-Bloch theorem, the equations of motion can be casted into the matrix form

$$\ddot{\mathbf{U}} + \mathbf{KU} + \mathbf{NL}_1 = \mathbf{0} \tag{4a}$$

$$\ddot{\mathbf{P}} + \chi_3 \mathbf{P} + \mathbf{NL}_2 = \mathbf{0} \tag{4b}$$

where variables $\mathbf{U} = [u_{3j} \ u_{3j+1} \ u_{3j+2}]^T$, $\mathbf{P} = [p_{3j} \ p_{3j+1} \ p_{3j+2}]^T$, and

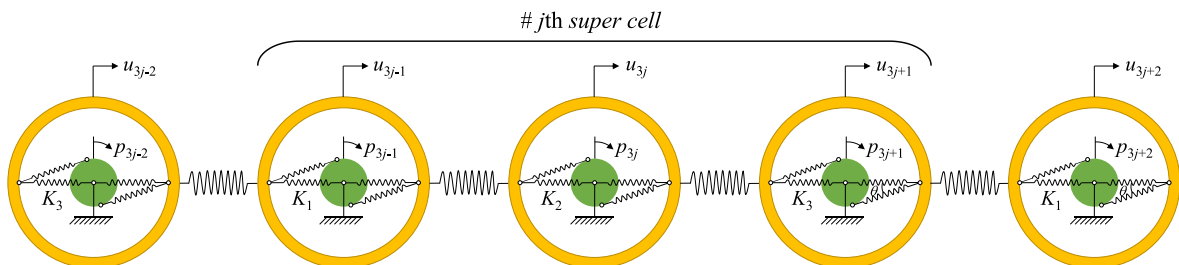


Fig. 2. Schematic of autoparametric modulated super cell.

$$\mathbf{K} = \begin{bmatrix} 2 + \lambda_1 & -1 & -e^{-i\xi} \\ -1 & 2 + \lambda_2 & -1 \\ -e^{i\xi} & -1 & 2 + \lambda_3 \end{bmatrix}, \mathbf{NL}_1 = \begin{bmatrix} \chi_2 p_{3j} u_{3j} \\ \chi_2 p_{3j+1} u_{3j+1} \\ \chi_2 p_{3j+2} u_{3j+2} \end{bmatrix}, \mathbf{NL}_2 = \begin{bmatrix} \chi_4 u_{3j}^2 \\ \chi_4 u_{3j+1}^2 \\ \chi_4 u_{3j+2}^2 \end{bmatrix} \tag{5}$$

with

$$\lambda_n = 2(\beta_n + a \cos^2 \theta), \beta_n = \frac{K_n}{k}, \chi_2 = 2a \tan \theta \sin^2 \theta, \chi_3 = \frac{2\alpha}{\mu}, \chi_4 = \frac{a \tan \theta \sin^2 \theta}{\mu \gamma^2} \tag{6}$$

Herein, ξ is the wavenumber of the propagation mode, index $n = 1, 2, 3$. The second-order multiple-time scales perturbation method is then utilized to capture the coupling effect between the vibration of chiral rotational disks and wave propagation in the lattice chain. It is noteworthy that, in the present study, we directly invoke the Floquet-Bloch theorem on the nonlinear wave system to obtain the nonlinear dynamical equations (4) governing the nonlinear dynamics of the autoparametric modulated super cell structure, and thereafter multiple-time scales perturbation technique will be applied to such nonlinear dynamical system to derive the evolution equations. In fact, we have verified that, the obtained evolution equations based on such analysis strategy is exactly the same as that from first applying multiple-time scales perturbation to the original nonlinear problem and then subsequently invoking the Floquet-Bloch theorem on each order linearized problem. The analysis strategy provided by the present study can also be applied to analyze other nonlinear wave dynamics of discrete lattices in which the nonlinearity stemming from on-site, such as metamaterials with nonlinear local resonance [35] and nonlinear inertia-induced autoparametric periodic structures [36]. However, when the nonlinearity comes from inter-site, for instance, phononic crystals with nonlinear internal force between two adjacent unit cell [37], the errors result if the Floquet-Bloch theorem is directly invoked on the original nonlinear equations of motion. In addition, based on the previous experience of analytical analysis on nonlinear dynamical systems with quadratic nonlinearity, at least second-order multiple-time scales perturbation should be employed to seize the harmonic content and the time evolution of amplitude and phase unless one to two internal resonance scenario is considered [38]. The theoretical study on the higher-order dispersion in nonlinear monoatomic and diatomic systems also indicated that the quadratic nonlinearity does not result in the shifting of frequency until second-order correction is considered [39]. Thus, the approximate solutions of Eq. (4) are sought in the perturbed form [40]

$$\mathbf{U}(\tau; \varepsilon) = \varepsilon \mathbf{U}_1(T_0, T_1, T_2) + \varepsilon^2 \mathbf{U}_2(T_0, T_1, T_2) + \varepsilon^3 \mathbf{U}_3(T_0, T_1, T_2) \tag{7a}$$

$$\mathbf{P}(\tau; \varepsilon) = \varepsilon \mathbf{P}_1(T_0, T_1, T_2) + \varepsilon^2 \mathbf{P}_2(T_0, T_1, T_2) + \varepsilon^3 \mathbf{P}_3(T_0, T_1, T_2) \tag{7b}$$

where ε is treated as a small perturbation parameter, the original time variable τ has been replaced by three variables representing different time scales, that is, $T_0 = \tau$, $T_1 = \varepsilon \tau$ and $T_2 = \varepsilon^2 \tau$. Displacement functions \mathbf{U}_n and \mathbf{P}_n with $n = 1, 2, 3$ are expressed to first-order, second-order and third-order in the form of perturbation, and

$$\mathbf{U}_n = \begin{bmatrix} u_{3j,n} \\ u_{3j+1,n} \\ u_{3j+2,n} \end{bmatrix}, \mathbf{P}_n = \begin{bmatrix} p_{3j,n} \\ p_{3j+1,n} \\ p_{3j+2,n} \end{bmatrix} \tag{8}$$

Substituting (7) into (4) and equating coefficients of like powers of ε , we obtain the following hierarchy of equations

Order ε^1

$$\frac{\partial^2 \mathbf{U}_1}{\partial T_0^2} + \mathbf{K} \mathbf{U}_1 = \mathbf{0} \tag{9a}$$

$$\frac{\partial^2 \mathbf{P}_1}{\partial T_0^2} + \chi_3 \mathbf{P}_1 = \mathbf{0} \tag{9b}$$

Order ε^2

$$\frac{\partial^2 \mathbf{U}_2}{\partial T_0^2} + \mathbf{K} \mathbf{U}_2 = -2 \frac{\partial^2 \mathbf{U}_1}{\partial T_0 \partial T_1} - \mathbf{NL}_{1,1} \tag{10a}$$

$$\frac{\partial^2 \mathbf{P}_2}{\partial T_0^2} + \chi_3 \mathbf{P}_2 = -2 \frac{\partial^2 \mathbf{P}_1}{\partial T_0 \partial T_1} - \mathbf{NL}_{2,1} \tag{10b}$$

Order ε^3

$$\frac{\partial^2 \mathbf{U}_3}{\partial T_0^2} + \mathbf{K} \mathbf{U}_3 = -2 \frac{\partial^2 \mathbf{U}_2}{\partial T_0 \partial T_1} - 2 \frac{\partial^2 \mathbf{U}_1}{\partial T_0 \partial T_2} - \frac{\partial^2 \mathbf{U}_1}{\partial T_1^2} - \mathbf{NL}_{1,2} \tag{11a}$$

$$\frac{\partial^2 \mathbf{P}_3}{\partial T_0^2} + \chi_3 \mathbf{P}_3 = -2 \frac{\partial^2 \mathbf{P}_2}{\partial T_0 \partial T_1} - 2 \frac{\partial^2 \mathbf{P}_1}{\partial T_0 \partial T_2} - \frac{\partial^2 \mathbf{P}_1}{\partial T_1^2} - \mathbf{NL}_{2,2} \tag{11b}$$

where

$$\begin{aligned}
 \mathbf{NL}_{1,1} &= \begin{bmatrix} \chi_2 p_{3j,1} u_{3j,1} \\ \chi_2 p_{3j+1,1} u_{3j+1,1} \\ \chi_2 p_{3j+2,1} u_{3j+2,1} \end{bmatrix}, \quad \mathbf{NL}_{2,1} = \begin{bmatrix} \chi_4 u_{3j,1}^2 \\ \chi_4 u_{3j+1,1}^2 \\ \chi_4 u_{3j+2,1}^2 \end{bmatrix}, \\
 \mathbf{NL}_{1,2} &= \begin{bmatrix} \chi_2 (p_{3j,2} u_{3j,1} + p_{3j,1} u_{3j,2}) \\ \chi_2 (p_{3j+1,2} u_{3j+1,1} + p_{3j+1,1} u_{3j+1,2}) \\ \chi_2 (p_{3j+2,2} u_{3j+2,1} + p_{3j+2,1} u_{3j+2,2}) \end{bmatrix}, \quad \mathbf{NL}_{2,2} = \begin{bmatrix} 2\chi_4 u_{3j,2} u_{3j,1} \\ 2\chi_4 u_{3j+1,2} u_{3j+1,1} \\ 2\chi_4 u_{3j+2,2} u_{3j+2,1} \end{bmatrix} \tag{12}
 \end{aligned}$$

It should be noted that, instead of introducing the perturbation parameter ϵ into the governing equations (4) in advance, we naturally separate the equations in each hierarchy by substituting the assumed approximate perturbation solutions (7) (starting from the first power of ϵ) into (4). Such procedure leads to the hierarchy index taking 1 on the linearized equation (9), and increasing progressively.

In the following calculations, general solutions to (9) are first determined and then substituted into (10) to resolve for \mathbf{U}_2 and \mathbf{P}_2 . Subsequently, solutions to (9) and (10) allow us to obtain the evolution equations describing the dynamics of wave-vibration coupling on a slower time scale.

The solutions of Eq. (9a) can be written in the usual form

$$\mathbf{U}_1^w = \mathbf{v} \mathbf{A} e^{i(j\xi - \omega T_0)} \tag{13}$$

where $\mathbf{v} = [v_1 \ v_2 \ v_3]^T$ are constants to be determined with the initial conditions, and ω is the angular frequency of the propagation mode. Inserting (13) into (9a) yields the following matrix equation

$$(\mathbf{K} - \omega^2 \mathbf{I}) \mathbf{v} = 0 \tag{14}$$

where \mathbf{I} represents the unity matrix.

Equation (14) admits three non-trivial solutions when the determinant of the matrix vanishes, i.e.,

$$D(\omega) = |\mathbf{K} - \omega^2 \mathbf{I}| = 0 \tag{15}$$

Then the general solution of first-order equation (9) can be expressed as a superposition of modes

$$\mathbf{U}_1 = \mathbf{v}_1 \mathbf{A}_1 e^{i(j\xi - \omega_1 T_0)} + \mathbf{v}_2 \mathbf{A}_2 e^{i(j\xi - \omega_2 T_0)} + \mathbf{v}_3 \mathbf{A}_3 e^{i(j\xi - \omega_3 T_0)} + \mathbf{v}_1 \bar{\mathbf{A}}_1 e^{-i(j\xi - \omega_1 T_0)} + \mathbf{v}_2 \bar{\mathbf{A}}_2 e^{-i(j\xi - \omega_2 T_0)} + \mathbf{v}_3 \bar{\mathbf{A}}_3 e^{-i(j\xi - \omega_3 T_0)} \tag{16a}$$

$$\mathbf{P}_1 = \begin{bmatrix} B_1 e^{i\Omega T_0} + \bar{B}_1 e^{-i\Omega T_0} \\ B_2 e^{i\Omega T_0} + \bar{B}_2 e^{-i\Omega T_0} \\ B_3 e^{i\Omega T_0} + \bar{B}_3 e^{-i\Omega T_0} \end{bmatrix} \tag{16b}$$

where A_n and B_n are both complex-valued functions with respect to the time scales T_1 and T_2 , and overbars represent the complex conjugates. The frequency of rotational vibration in each sub cell is equal, expressed as $\Omega = \sqrt{\chi_3}$. Matrix \mathbf{v}_n satisfy the equation $(\mathbf{K} - \omega_n^2 \mathbf{I}) \mathbf{v}_n = 0$. Without loss of generality, \mathbf{v}_n can be expressed as

$$\begin{aligned}
 \mathbf{v}_1 &= \begin{bmatrix} 1 \\ v_{21} \\ v_{31} \end{bmatrix}, \quad \mathbf{v}_2 = \begin{bmatrix} 1 \\ v_{22} \\ v_{32} \end{bmatrix}, \quad \mathbf{v}_3 = \begin{bmatrix} 1 \\ v_{23} \\ v_{33} \end{bmatrix}, \quad v_{2n} = \frac{2 + \lambda_1 - \omega_n^2 + e^{-i\xi}}{1 + e^{-i\xi} (2 + \lambda_2 - \omega_n^2)}, \\
 v_{3n} &= \frac{\omega_n^4 - \lambda_1 \omega_n^2 - \lambda_2 \omega_n^2 - 4\omega_n^2 + \lambda_1 \lambda_2 + 2\lambda_1 + 2\lambda_2 + 3}{1 + e^{-i\xi} (2 + \lambda_2 - \omega_n^2)} \tag{17}
 \end{aligned}$$

Substituting solutions (16) into (10), and setting the secular terms containing $e^{\pm i(j\xi - \omega_n T_0)}$ in (10a) and $e^{\pm i\Omega T_0}$ in (10b) to be zero, yields

$$\frac{\partial A_n}{\partial T_1} = 0, \quad \frac{\partial B_n}{\partial T_1} = 0 \tag{18}$$

We note that amplitudes A_n and B_n only depend on the time scales T_2 . Meanwhile, the particular solutions of second-order equation (10) are sought in the following form

$$\begin{aligned}
 \mathbf{U}_2 = & \mathbf{E}^1 A_1 B_1 e^{i(j\xi - \omega_1 T_0 + \Omega T_0)} + \mathbf{E}^2 A_1 \bar{B}_1 e^{i(j\xi - \omega_1 T_0 - \Omega T_0)} + \mathbf{E}^3 A_2 B_1 e^{i(j\xi - \omega_2 T_0 + \Omega T_0)} \\
 & + \mathbf{E}^4 A_2 \bar{B}_1 e^{i(j\xi - \omega_2 T_0 - \Omega T_0)} + \mathbf{E}^5 A_3 B_1 e^{i(j\xi - \omega_3 T_0 + \Omega T_0)} + \mathbf{E}^6 A_3 \bar{B}_1 e^{i(j\xi - \omega_3 T_0 - \Omega T_0)} \\
 & + \mathbf{E}^7 \bar{A}_1 B_1 e^{i(\omega_1 T_0 - j\xi + \Omega T_0)} + \mathbf{E}^8 \bar{A}_1 \bar{B}_1 e^{i(\omega_1 T_0 - \Omega T_0 - j\xi)} + \mathbf{E}^9 \bar{A}_2 B_1 e^{i(\omega_2 T_0 - j\xi + \Omega T_0)} \\
 & + \mathbf{E}^{10} \bar{A}_2 \bar{B}_1 e^{i(\omega_2 T_0 - j\xi - \Omega T_0)} + \mathbf{E}^{11} \bar{A}_3 B_1 e^{i(\omega_3 T_0 - j\xi + \Omega T_0)} + \mathbf{E}^{12} \bar{A}_3 \bar{B}_1 e^{i(\omega_3 T_0 - j\xi - \Omega T_0)} \\
 & + \mathbf{E}^{13} A_1 B_2 e^{i(j\xi - \omega_1 T_0 + \Omega T_0)} + \mathbf{E}^{14} A_1 \bar{B}_2 e^{i(j\xi - \omega_1 T_0 - \Omega T_0)} + \mathbf{E}^{15} A_2 B_2 e^{i(j\xi - \omega_2 T_0 + \Omega T_0)} \\
 & + \mathbf{E}^{16} A_2 \bar{B}_2 e^{i(j\xi - \omega_2 T_0 - \Omega T_0)} + \mathbf{E}^{17} A_3 B_2 e^{i(j\xi - \omega_3 T_0 + \Omega T_0)} + \mathbf{E}^{18} A_3 \bar{B}_2 e^{i(j\xi - \omega_3 T_0 - \Omega T_0)} \\
 & + \mathbf{E}^{19} \bar{A}_1 B_2 e^{i(\omega_1 T_0 - j\xi + \Omega T_0)} + \mathbf{E}^{20} \bar{A}_1 \bar{B}_2 e^{i(\omega_1 T_0 - \Omega T_0 - j\xi)} + \mathbf{E}^{21} \bar{A}_2 B_2 e^{i(\omega_2 T_0 - j\xi + \Omega T_0)} \\
 & + \mathbf{E}^{22} \bar{A}_2 \bar{B}_2 e^{i(\omega_2 T_0 - j\xi - \Omega T_0)} + \mathbf{E}^{23} \bar{A}_3 B_2 e^{i(\omega_3 T_0 - j\xi + \Omega T_0)} + \mathbf{E}^{24} \bar{A}_3 \bar{B}_2 e^{i(\omega_3 T_0 - j\xi - \Omega T_0)} \\
 & + \mathbf{E}^{25} A_1 B_3 e^{i(j\xi - \omega_1 T_0 + \Omega T_0)} + \mathbf{E}^{26} A_1 \bar{B}_3 e^{i(j\xi - \omega_1 T_0 - \Omega T_0)} + \mathbf{E}^{27} A_2 B_3 e^{i(j\xi - \omega_2 T_0 + \Omega T_0)} \\
 & + \mathbf{E}^{28} A_2 \bar{B}_3 e^{i(j\xi - \omega_2 T_0 - \Omega T_0)} + \mathbf{E}^{29} A_3 B_3 e^{i(j\xi - \omega_3 T_0 + \Omega T_0)} + \mathbf{E}^{30} A_3 \bar{B}_3 e^{i(j\xi - \omega_3 T_0 - \Omega T_0)} \\
 & + \mathbf{E}^{31} \bar{A}_1 B_3 e^{i(\omega_1 T_0 - j\xi + \Omega T_0)} + \mathbf{E}^{32} \bar{A}_1 \bar{B}_3 e^{i(\omega_1 T_0 - \Omega T_0 - j\xi)} + \mathbf{E}^{33} \bar{A}_2 B_3 e^{i(\omega_2 T_0 - j\xi + \Omega T_0)} \\
 & + \mathbf{E}^{34} \bar{A}_2 \bar{B}_3 e^{i(\omega_2 T_0 - j\xi - \Omega T_0)} + \mathbf{E}^{35} \bar{A}_3 B_3 e^{i(\omega_3 T_0 - j\xi + \Omega T_0)} + \mathbf{E}^{36} \bar{A}_3 \bar{B}_3 e^{i(\omega_3 T_0 - j\xi - \Omega T_0)}
 \end{aligned} \tag{19a}$$

$$\begin{aligned}
 \mathbf{P}_2 = & \mathbf{F}^1 A_1^2 e^{2i(j\xi - \omega_1 T_0)} + \mathbf{F}^2 A_1 A_2 e^{i(2j\xi - \omega_2 T_0 - \omega_1 T_0)} + \mathbf{F}^3 A_1 A_3 e^{i(2j\xi - \omega_3 T_0 - \omega_1 T_0)} + \mathbf{F}^4 A_1 \bar{A}_1 \\
 & + \mathbf{F}^5 A_1 \bar{A}_2 e^{i(\omega_2 T_0 - \omega_1 T_0)} + \mathbf{F}^6 A_1 \bar{A}_3 e^{i(\omega_3 T_0 - \omega_1 T_0)} + \mathbf{F}^7 A_2^2 e^{2i(j\xi - \omega_2 T_0)} + \mathbf{F}^{10} A_2 \bar{A}_2 \\
 & + \mathbf{F}^8 A_3 A_2 e^{i(2j\xi - \omega_2 T_0 - \omega_3 T_0)} + \mathbf{F}^9 \bar{A}_1 A_2 e^{i(\omega_1 T_0 - \omega_2 T_0)} + \mathbf{F}^{11} \bar{A}_3 A_2 e^{i(\omega_3 T_0 - \omega_2 T_0)} \\
 & + \mathbf{F}^{12} A_3^2 e^{2i(j\xi - \omega_3 T_0)} + \mathbf{F}^{13} \bar{A}_1 A_3 e^{i(\omega_1 T_0 - \omega_3 T_0)} + \mathbf{F}^{14} A_3 \bar{A}_2 e^{i(\omega_2 T_0 - \omega_3 T_0)} + \mathbf{F}^{15} A_3 \bar{A}_3 \\
 & + \mathbf{F}^{16} \bar{A}_1^2 e^{-2i(j\xi - \omega_1 T_0)} + \mathbf{F}^{17} \bar{A}_1 \bar{A}_2 e^{-i(2j\xi - \omega_2 T_0 - \omega_1 T_0)} + \mathbf{F}^{18} \bar{A}_1 \bar{A}_3 e^{-i(2j\xi - \omega_3 T_0 - \omega_1 T_0)} \\
 & + \mathbf{F}^{19} \bar{A}_2^2 e^{-2i(j\xi - \omega_2 T_0)} + \mathbf{F}^{20} \bar{A}_3 \bar{A}_2 e^{-i(2j\xi - \omega_2 T_0 - \omega_3 T_0)} + \mathbf{F}^{21} \bar{A}_3^2 e^{-2i(j\xi - \omega_3 T_0)}
 \end{aligned} \tag{19b}$$

in which, matrices $\mathbf{E}^h = [e_{11}^h \ e_{21}^h \ e_{31}^h]^T$ ($h = 1, 2, \dots, 36$), $\mathbf{F}^g = [f_{11}^g \ f_{21}^g \ f_{31}^g]^T$ ($g = 1, 2, \dots, 21$), and all the parameters can be obtained by substituting (19) into (10) and balancing similar terms. Inserting (16) and (18–19) into (11) and eliminating the secular terms leads to

$$\begin{vmatrix} Q_n^1 & -1 & -e^{-i\xi} \\ Q_n^2 & 2 + \lambda_2 - \omega_n^2 & -1 \\ Q_n^3 & -1 & 2 + \lambda_3 - \omega_n^2 \end{vmatrix} = 0 \tag{20a}$$

$$2i\Omega \frac{\partial B_n}{\partial T_2} + \left(b_n^1 A_1 \bar{A}_1 + b_n^2 A_2 \bar{A}_2 + b_n^3 A_3 \bar{A}_3 \right) B_1 \tag{20b}$$

$$+ \left(b_n^4 A_1 \bar{A}_1 + b_n^5 A_2 \bar{A}_2 + b_n^6 A_3 \bar{A}_3 \right) B_2 + \left(b_n^7 A_1 \bar{A}_1 + b_n^8 A_2 \bar{A}_2 + b_n^9 A_3 \bar{A}_3 \right) B_3 = 0$$

where

$$\begin{aligned}
 Q_1^1 = & 2i\omega_1 \frac{\partial A_1}{\partial T_2} - \chi_2 (f_{11}^1 + f_{11}^4) A_1^2 \bar{A}_1 - \chi_2 (f_{11}^{10} + v_{12} f_{11}^2 + v_{12} f_{11}^5) A_1 A_2 \bar{A}_2 \\
 & - \chi_2 (f_{11}^{15} + v_{13} f_{11}^3 + v_{13} f_{11}^6) A_1 A_3 \bar{A}_3 - \chi_2 (e_{11}^1 + e_{11}^2) A_1 B_1 \bar{B}_1 \\
 & - \chi_2 e_{11}^{14} A_1 B_1 \bar{B}_2 - \chi_2 e_{11}^{26} A_1 B_1 \bar{B}_3 - \chi_2 e_{11}^{13} A_1 B_2 \bar{B}_1 - \chi_2 e_{11}^{25} A_1 B_3 \bar{B}_1,
 \end{aligned}$$

$$\begin{aligned}
 Q_1^2 = & 2iv_{21}\omega_1 \frac{\partial A_1}{\partial T_2} - \chi_2 v_{21} (f_{21}^1 + f_{21}^4) A_1^2 \bar{A}_1 - \chi_2 (v_{21} f_{21}^{10} + v_{22} f_{21}^2 + v_{22} f_{21}^5) A_1 A_2 \bar{A}_2 \\
 & - \chi_2 (v_{21} f_{21}^{15} + v_{23} f_{21}^3 + v_{23} f_{21}^6) A_1 A_3 \bar{A}_3 - \chi_2 (e_{21}^{13} + e_{21}^{14}) A_1 B_2 \bar{B}_2 \\
 & - \chi_2 e_{21}^1 A_1 B_1 \bar{B}_2 - \chi_2 e_{21}^{25} A_1 B_3 \bar{B}_2 - \chi_2 e_{21}^{26} A_1 B_2 \bar{B}_3 - \chi_2 e_{21}^2 A_1 B_2 \bar{B}_1,
 \end{aligned}$$

$$\begin{aligned}
 Q_1^3 = & 2iv_{31}\omega_1 \frac{\partial A_1}{\partial T_2} - v_{31}\chi_2 (f_{31}^1 + f_{31}^4) A_1^2 \bar{A}_1 - \chi_2 (v_{31} f_{31}^{10} + v_{32} f_{31}^2 + v_{32} f_{31}^5) A_1 A_2 \bar{A}_2 \\
 & - \chi_2 (v_{31} f_{31}^{15} + v_{33} f_{31}^3 + v_{33} f_{31}^6) A_1 A_3 \bar{A}_3 - \chi_2 (e_{31}^{25} + e_{31}^{26}) A_1 B_3 \bar{B}_3 \\
 & - \chi_2 e_{31}^1 A_1 B_1 \bar{B}_3 - \chi_2 e_{31}^{14} A_1 B_3 \bar{B}_2 - \chi_2 e_{31}^{13} A_1 B_2 \bar{B}_3 - \chi_2 e_{31}^2 A_1 B_3 \bar{B}_1,
 \end{aligned}$$

$$\begin{aligned}
 Q_2^1 = & 2i\omega_2 \frac{\partial A_2}{\partial T_2} - \chi_2 (f_{11}^{10} + f_{11}^7) A_2^2 \bar{A}_2 - \chi_2 (f_{11}^4 + f_{11}^2 + f_{11}^9) A_2 A_1 \bar{A}_1 \\
 & - \chi_2 (f_{11}^{15} + f_{11}^1 + f_{11}^8) A_2 A_3 \bar{A}_3 - \chi_2 (e_{11}^3 + e_{11}^4) A_2 B_1 \bar{B}_1 \\
 & - \chi_2 e_{11}^{16} A_2 B_1 \bar{B}_2 - \chi_2 e_{11}^{28} A_2 B_1 \bar{B}_3 - \chi_2 e_{11}^{15} A_2 B_2 \bar{B}_1 - \chi_2 e_{11}^{27} A_2 B_3 \bar{B}_1,
 \end{aligned}$$

$$Q_2^2 = 2i\omega_2 v_{22} \frac{\partial A_2}{\partial T_2} - \chi_2 v_{22} (f_{21}^{10} + f_{21}^7) A_2^2 \bar{A}_2 - \chi_2 (v_{22} f_{21}^4 + v_{21} f_{21}^2 + v_{21} f_{21}^9) A_2 A_1 \bar{A}_1 - \chi_2 (v_{22} f_{21}^{15} + v_{23} f_{21}^{11} + v_{23} f_{21}^8) A_2 A_3 \bar{A}_3 - \chi_2 (e_{21}^{15} + e_{21}^{16}) A_2 B_2 \bar{B}_2 - \chi_2 e_{21}^3 A_2 B_1 \bar{B}_2 - \chi_2 e_{21}^{27} A_2 B_3 \bar{B}_2 - \chi_2 e_{21}^{28} A_2 B_2 \bar{B}_3 - \chi_2 e_{21}^4 A_2 B_2 \bar{B}_1,$$

$$Q_2^3 = 2i\omega_2 v_{32} \frac{\partial A_2}{\partial T_2} - \chi_2 v_{32} (f_{31}^{10} + f_{31}^7) A_2^2 \bar{A}_2 - \chi_2 (v_{32} f_{31}^4 + v_{31} f_{31}^2 + v_{31} f_{31}^9) A_2 A_1 \bar{A}_1 - \chi_2 (v_{32} f_{31}^{15} + v_{33} f_{31}^{11} + v_{33} f_{31}^8) A_2 A_3 \bar{A}_3 - \chi_2 (e_{31}^{27} + e_{31}^{28}) A_2 B_3 \bar{B}_3 - \chi_2 e_{31}^3 A_2 B_1 \bar{B}_3 - \chi_2 e_{31}^{16} A_2 B_3 \bar{B}_2 - \chi_2 e_{31}^{15} A_2 B_2 \bar{B}_3 - \chi_2 e_{31}^4 A_2 B_3 \bar{B}_1,$$

$$Q_3^1 = 2i\omega_3 \frac{\partial A_3}{\partial T_2} - \chi_2 (f_{11}^{12} + f_{11}^{15}) A_3^2 \bar{A}_3 - \chi_2 (f_{11}^{10} + f_{11}^{14} + f_{11}^8) A_3 A_2 \bar{A}_2 - \chi_2 (f_{11}^{13} + f_{11}^3 + f_{11}^4) A_3 A_1 \bar{A}_1 - \chi_2 (e_{11}^5 + e_{11}^6) A_3 B_1 \bar{B}_1 - \chi_2 e_{11}^{18} A_3 B_1 \bar{B}_2 - \chi_2 e_{11}^{30} A_3 B_1 \bar{B}_3 - \chi_2 e_{11}^{17} A_3 B_2 \bar{B}_1 - \chi_2 e_{11}^{29} A_3 B_3 \bar{B}_1,$$

$$Q_3^2 = 2i\omega_3 v_{23} \frac{\partial A_3}{\partial T_2} - \chi_2 v_{23} (f_{21}^{12} + f_{21}^{15}) A_3^2 \bar{A}_3 - \chi_2 (v_{23} f_{21}^{10} + v_{22} f_{21}^{14} + v_{22} f_{21}^8) A_3 A_2 \bar{A}_2 - \chi_2 (v_{21} f_{21}^{13} + v_{21} f_{21}^3 + v_{23} f_{21}^4) A_3 A_1 \bar{A}_1 - \chi_2 (e_{21}^{17} + e_{21}^{18}) A_3 B_2 \bar{B}_2 - \chi_2 e_{21}^5 A_3 B_1 \bar{B}_2 - \chi_2 e_{21}^{29} A_3 B_3 \bar{B}_2 - \chi_2 e_{21}^{30} A_3 B_2 \bar{B}_3 - \chi_2 e_{21}^6 A_3 B_2 \bar{B}_1,$$

$$Q_3^3 = 2i\omega_3 v_{33} \frac{\partial A_3}{\partial T_2} - \chi_2 v_{33} (f_{31}^{12} + f_{31}^{15}) A_3^2 \bar{A}_3 - \chi_2 (v_{33} f_{31}^{10} + v_{32} f_{31}^{14} + v_{32} f_{31}^8) A_3 A_2 \bar{A}_2 - \chi_2 (v_{31} f_{31}^{13} + v_{31} f_{31}^3 + v_{33} f_{31}^4) A_3 A_1 \bar{A}_1 - \chi_2 (e_{31}^{29} + e_{31}^{30}) A_3 B_3 \bar{B}_3 - \chi_2 e_{31}^5 A_3 B_1 \bar{B}_3 - \chi_2 e_{31}^{18} A_3 B_3 \bar{B}_2 - \chi_2 e_{31}^{17} A_3 B_2 \bar{B}_3 - \chi_2 e_{31}^6 A_3 B_3 \bar{B}_1,$$

$$b_1^1 = 2\chi_4 (e_{11}^1 + e_{11}^7), b_1^2 = 2\chi_4 v_{12} (e_{11}^3 + e_{11}^9), b_1^3 = 2\chi_4 v_{13} (e_{11}^5 + e_{11}^{11}),$$

$$b_1^4 = 2\chi_4 (e_{11}^{13} + e_{11}^{19}), b_1^5 = 2\chi_4 v_{12} (e_{11}^{15} + e_{11}^{21}), b_1^6 = 2\chi_4 v_{13} (e_{11}^{17} + e_{11}^{23}),$$

$$b_1^7 = 2\chi_4 (e_{11}^{25} + e_{11}^{31}), b_1^8 = 2\chi_4 v_{12} (e_{11}^{27} + e_{11}^{33}), b_1^9 = 2\chi_4 v_{13} (e_{11}^{29} + e_{11}^{35}),$$

$$b_2^1 = 2\chi_4 (e_{21}^1 + e_{21}^7), b_2^2 = 2\chi_4 v_{22} (e_{21}^3 + e_{21}^9), b_2^3 = 2\chi_4 v_{23} (e_{21}^5 + e_{21}^{11}),$$

$$b_2^4 = 2\chi_4 (e_{21}^{13} + e_{21}^{19}), b_2^5 = 2\chi_4 v_{22} (e_{21}^{15} + e_{21}^{21}), b_2^6 = 2\chi_4 v_{23} (e_{21}^{17} + e_{21}^{23}),$$

$$b_2^7 = 2\chi_4 (e_{21}^{25} + e_{21}^{31}), b_2^8 = 2\chi_4 v_{22} (e_{21}^{27} + e_{21}^{33}), b_2^9 = 2\chi_4 v_{23} (e_{21}^{29} + e_{21}^{35}),$$

$$b_3^1 = 2\chi_4 (e_{31}^1 + e_{31}^7), b_3^2 = 2\chi_4 v_{32} (e_{31}^3 + e_{31}^9), b_3^3 = 2\chi_4 v_{33} (e_{31}^5 + e_{31}^{11}),$$

$$b_3^4 = 2\chi_4 (e_{31}^{13} + e_{31}^{19}), b_3^5 = 2\chi_4 v_{32} (e_{31}^{15} + e_{31}^{21}), b_3^6 = 2\chi_4 v_{33} (e_{31}^{17} + e_{31}^{23}),$$

$$b_3^7 = 2\chi_4 (e_{31}^{25} + e_{31}^{31}), b_3^8 = 2\chi_4 v_{32} (e_{31}^{27} + e_{31}^{33}), b_3^9 = 2\chi_4 v_{33} (e_{31}^{29} + e_{31}^{35}) \tag{21}$$

Rewriting $A_n = A_{0n} e^{i\phi_n(T_2)}/2$ and $B_n = B_{0n} e^{i\phi_n(T_2)}/2$ in (20), we obtain the following evolution equations

$$\frac{\partial A_{0n}}{\partial T_2} = \frac{1}{2} A_{0n} Im(\Delta_n^1) \tag{22a}$$

$$\frac{\partial B_{0n}}{\partial T_2} = -\frac{1}{\Omega} Im(\Delta_n^2) \tag{22b}$$

$$\frac{\partial \Phi_n}{\partial T_2} = -\frac{1}{2} Re(\Delta_n^1) \tag{22c}$$

$$\frac{\partial \phi_n}{\partial T_2} = \frac{1}{\Omega B_{0n}} Re(\Delta_n^2) \tag{22d}$$

where

$$\begin{aligned} \Delta_n^1 &= \frac{1}{4} (g_n^1 A_{01}^2 + g_n^2 A_{02}^2 + g_n^3 A_{03}^2 + g_n^4 B_{01}^2 + g_n^5 B_{01} B_{02} e^{i(\phi_1 - \phi_2)} + g_n^6 B_{01} B_{03} e^{i(\phi_1 - \phi_3)} + g_n^7 B_{02} B_{01} e^{-i(\phi_1 - \phi_2)}) \\ &\quad + \frac{1}{4} (g_n^8 B_{03} B_{01} e^{-i(\phi_1 - \phi_3)} + g_n^9 B_{02}^2 + g_n^{10} B_{02} B_{03} e^{i(\phi_2 - \phi_3)} + g_n^{11} B_{03} B_{02} e^{-i(\phi_2 - \phi_3)} + g_n^{12} B_{03}^2), \\ \Delta_n^2 &= \frac{1}{8} [(b_n^1 A_{01}^2 + b_n^2 A_{02}^2 + b_n^3 A_{03}^2) B_{01} e^{-i\phi_1} + (b_n^4 A_{01}^2 + b_n^5 A_{02}^2 + b_n^6 A_{03}^2) B_{02} e^{-i\phi_2} \\ &\quad + (b_n^7 A_{01}^2 + b_n^8 A_{02}^2 + b_n^9 A_{03}^2) B_{03} e^{-i\phi_3}] e^{-i\phi_n} \end{aligned} \tag{23}$$

and parameters g_n^q ($q = 1, 2, \dots, 12$) can be obtained from equation (20a) by balancing similar terms.

By examination of Eq. (22a), it is apparent that a fixed point exists at $A_{0n} = 0$ and its stability is affected by the dynamical behavior of amplitude evolution which is finally determined by the frequency of rotational vibration. Inspection of high dimensional dynamical system (22) shows that the amplitude and phase of rotational vibration gradually tend to constants as the amplitude of longitudinal wave evolves towards the fixed point when a moderate modulated frequency of rotational vibration is considered, whereas, when a fast

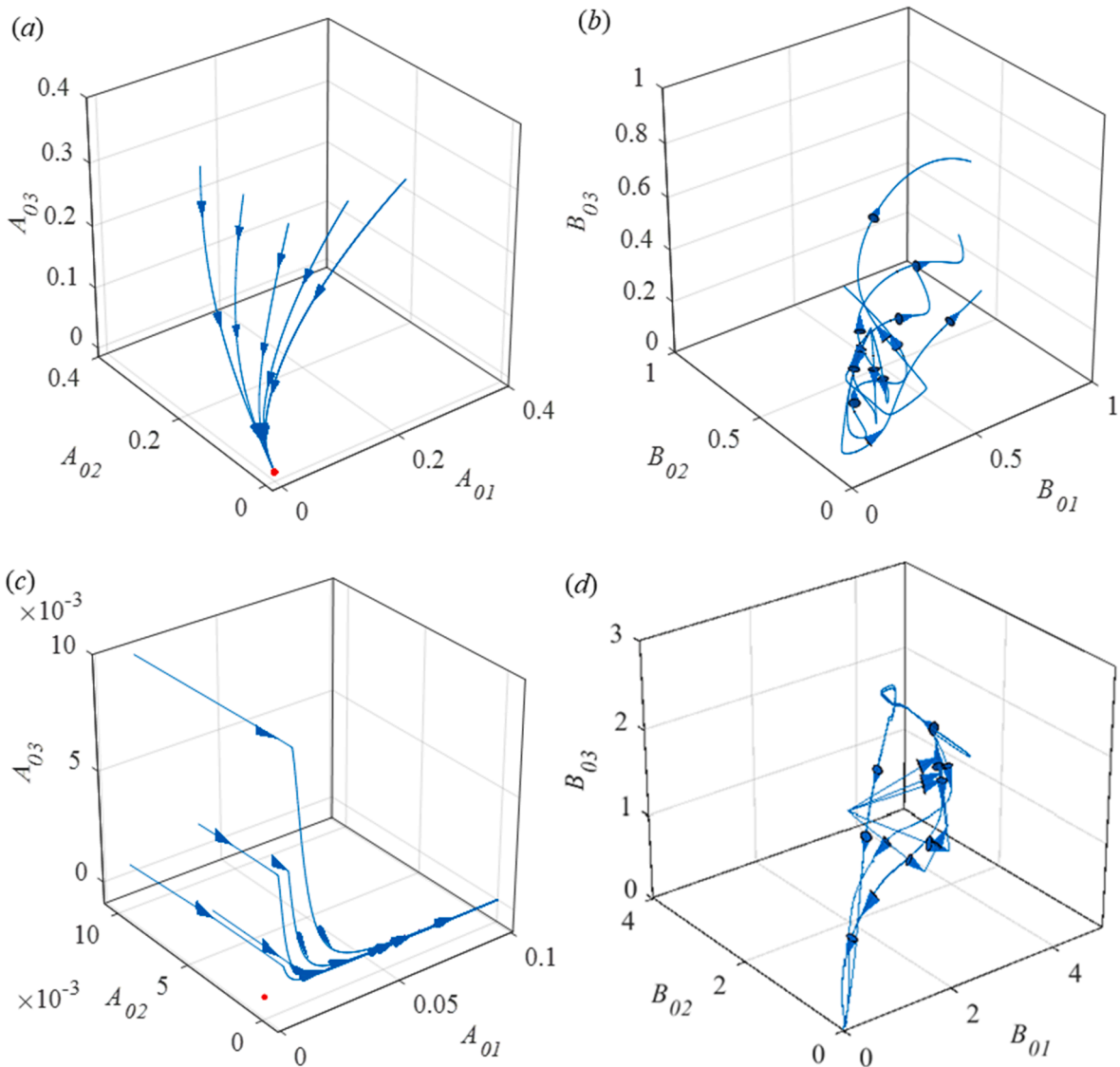


Fig. 3. The global dynamics flow in the projected amplitude A_{0n} space and B_{0n} space when the fixed point (red point) is stable (a) and (b), and unstable (c) and (d). (For interpretation of the references to colour in this figure legend, the reader is referred to the web version of this article.)

modulated frequency of rotational vibration is considered, the amplitude of longitudinal wave is amplified exponentially as the amplitude of rotational vibration evolves towards zero. Such evolution process is accompanied by energy transports between the longitudinal wave and the rotational vibration of our conservative autoparametric system. The projections of global evolution flow in three-dimensional amplitude space induced by the initial phases $\phi_n = -2\pi n/3$ of the vibratory disks are shown in Fig. 3 with the dimensionless parameters $\alpha = 0.75, \beta = [0.0167, 0.0833, 0.3333], \gamma = 0.1667, \mu = 4, \theta = 0.5236, \xi = 0.2094$ for the stable fixed point and parameters $\alpha = 0.75, \beta = [0.0167, 0.0833, 0.3333], \gamma = 0.1667, \mu = 0.12, \theta = 0.5236, \xi = 1.4392$ for the unstable fixed point. It is noteworthy that, the time-growing wave evolution is associated with the generation of unstable manifold when a supersonic modulated vibration is imposed. Such instable propagating wave can be created by the present autoparametric system and has wide applications on mechanical amplifications. On the other hand, when a subsonic modulated vibration is triggered, a one-way net power flow output produces from the longitudinal wave to the rotational vibration, which squeezes the finite amplitude of longitudinal wave to infinite small, the fixed point. At the fixed point, the rest equations of (22) can be reduced in the following form

$$\frac{\partial \Phi_n}{\partial T_2} = -\frac{1}{2} Re \left(\Delta_n^1 \Big|_{A_{01}=A_{02}=A_{03}=0} \right), \frac{\partial B_{0n}}{\partial T_2} = 0, \frac{\partial \phi_n}{\partial T_2} = 0 \tag{24}$$

In this scenario, the amplitude B_{0n} and phase ϕ_n of the vibratory disks for the n th sub cell is constant. Combining equations (7b), (16b), (19b) and (24), the approximate solutions of rotational vibration can be written as

$$\mathbf{P}(\tau; \varepsilon) = \begin{bmatrix} \varepsilon B_{01} \cos(\Omega \tau + \phi_1) \\ \varepsilon B_{02} \cos(\Omega \tau + \phi_2) \\ \varepsilon B_{03} \cos(\Omega \tau + \phi_3) \end{bmatrix} \tag{25}$$

In other words, when the amplitude of longitudinal wave is obviously smaller than that of the rotational vibration, the amplitude and phase of rotational vibration are not modulated by the longitudinal wave. The two-way coupling autoparametric modulated system will be degenerated to a one-way coupling system. Introducing an appropriate sequence of the initial phases of the vibratory disks can directly create the spatial waveform of modulation. This is exactly the small-on-large coupling mechanism. Thus, we now know that the small-on-large effect can be readily constructed from an autoparametric system. Moreover, the phase evolution of longitudinal wave provides the second-order correction upon the linear wave frequency, and the band structure constantly used in wave analysis will continue to be valid to characterize the intrinsic characteristics of the autoparametric modulated system in the sense of small-on-large.

Revisiting the particular solution (19), it is worth noting that there are six kinds of denominators of the parameters \mathbf{E}^h , expressed as functions $D(\omega_1 \pm \Omega), D(\omega_2 \pm \Omega)$ and $D(\omega_3 \pm \Omega)$. These functions contain physical information about the possible resonance processes that underlie the nonlinear modes of our autoparametric system. A resonance may appear due to the vanishing of denominators at certain values of frequency-wavenumber pairs.

Returning to the original time scale, then, the second-order correction to the linear frequency is expressed as follows

$$\omega_n^{NL} = \omega_n + \frac{\varepsilon^2}{2} Re \left(\Delta_n^1 \Big|_{A_{01}=A_{02}=A_{03}=0} \right) \tag{26}$$

According to (26), the dispersion curves corresponding to the fundamental mode of Bloch waves can be tracked for each

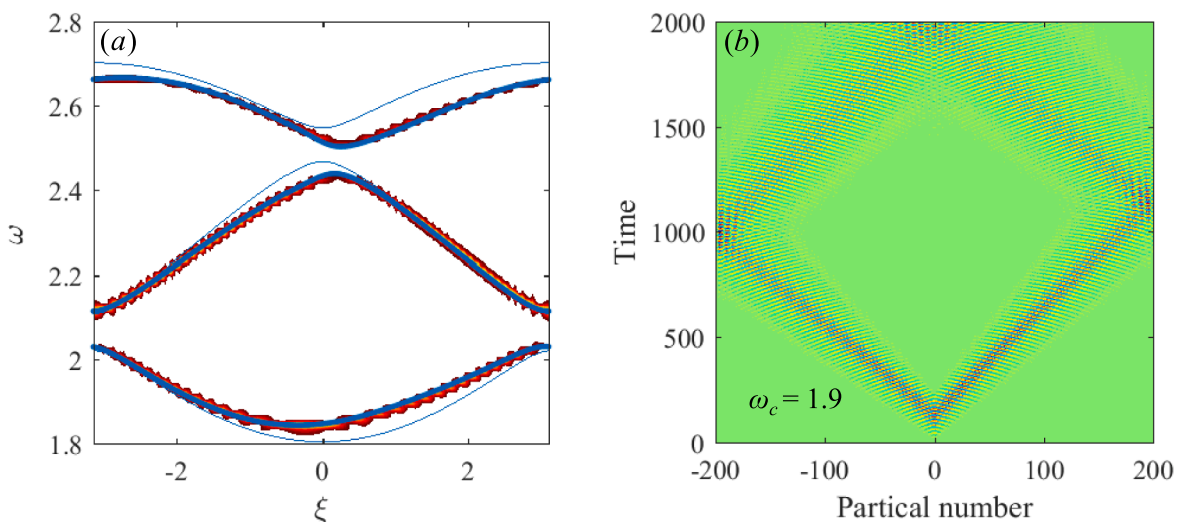


Fig. 4. (a) The dispersion curves of an autoparametric modulated structure obtained using full numerical simulations (level sets) compared to the one determined by the method of multiple-time scales with second-order accuracy (solid dots). (b) Spatiotemporal trajectory of partial displacement when signal is sent from the mid-span.

wavenumber. The effectiveness of the perturbation procedure will be verified by comparing analytical dispersion curves with those reconstructed from the direct numerical simulations, as addressed in the next section. It is worth to note, to characterize the non-reciprocal wave propagation of autoparametric systems, efforts might be also devoted to an asymptotic analysis based on coupled mode theory [15] applied to equations of motion (4). With separation of the incident wave dispersion branch C^0 and scattered ones $C^{\pm 1}$, the coupled mode theory based on first-order perturbation can explain the bandgaps generation induced by the autoparametric modulation when coupled modes exist, which we call, the moderate autoparametric modulation. However, it cannot take into account the asymmetry in dispersion curves where only single uncoupled mode exists, which we call, the fast autoparametric modulation. In view of this, higher-order coupled mode theory is worth developing for capturing such asymmetry.

4. Non-reciprocal effect in autoparametric periodic structure

This section is devoted to the analysis of the non-reciprocal effect of periodic structures with fast, moderate, and quasi-static autoparametric modulation, respectively. Classification of modulation speed is according to the magnitude of the rotational vibration frequency Ω .

4.1. Fast autoparametric modulation

Consider the case of the fast autoparametric modulation with $\Omega = 1$. Fig. 4 (a) shows by the thin solid line the dispersion diagram of the unmodulated structure, in which the geometrically linear deformation of inclined spring is considered such that the rotational vibration and the longitudinal wave are decoupled. The presence of the bandgap below a cut-off frequency ($\omega = 1.8$), the so-called the Drude dispersion behavior [41], arises from the constrained longitudinal movement of internal disks. Notice that such wide bandgap in the low frequency regime is intentionally not exhibited in order to highlight the features of non-reciprocity. The band diagram for the unmodulated structure is seen to follow the mirror symmetry in the wave vector space as the preservation of time reversal symmetry. For the modulated structure with the nonlinear mode coupling, the fundamental dispersion branch is calculated by the perturbation method as plotted by the solid dots in Fig. 4 (a). It is noteworthy that this asymmetry in dispersion curves can be easily observed in the case of fast autoparametric modulation and predicted by the method of multiple-time scales with second-order accuracy, but cannot be captured based on coupled mode theory.

To validate the analytical dispersion relations, we perform transient numerical simulations for the proposed nonlinear chiral-induced autoparametric periodic structure with internal wave-like modulation. The simulation model of the 1D chain contains 401 cells with the dimensionless parameters: $\alpha = 2$, $\beta = [0.0167, 0.0833, 0.3333]$, $\gamma = 0.1667$, $\mu = 4$, $\theta = 0.5236$, and the amplitude B_{0n} of the initial rotational vibration is set as 0.7π . The displacement excitation characterized by the broadband tone burst signal of the form $A[H(\tau) - H(\tau - N/f_c)] [1 - \cos(\omega_c \tau/N)] \sin(\omega_c \tau)$ is imposed at the middle of the chain, where A is an amplitude, H is the Heaviside function, ω_c is the central frequency, and N is the number of cycles. The time-domain displacement responses in spatial lattice points away from the excitation location are Fourier-transformed to reconstruct the dispersion diagram as shown by the contour plot in Fig. 4 (a). By comparing the numerical dispersion contours and analytical results, the perturbation methodology for the estimation of the dispersion diagrams can be verified. To further demonstrate the non-reciprocal wave behavior, the transient displacement response to the narrow-band pulse excitation centered at $\omega_c = 1.9$ within the pass band of Fig. 4 (a) is computed, as shown in Fig. 4 (b). Distinct

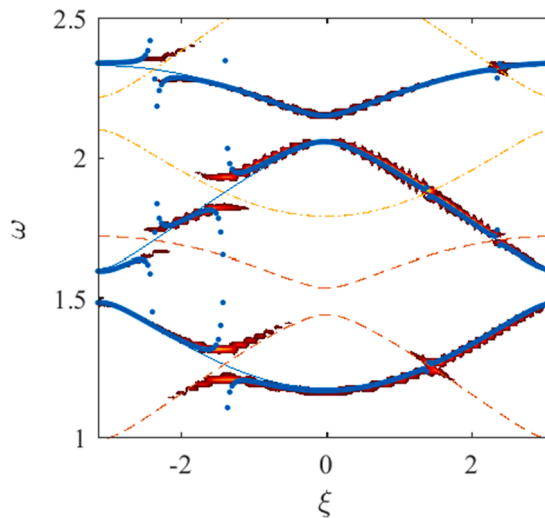


Fig. 5. The dispersion curves of an autoparametric modulated structure obtained using full numerical simulations (level sets) compared to the one determined by the method of multiple-time scales with second-order accuracy (solid dots). The incident wave dispersion branch C^0 is represented by the thin solid lines, and the scattered wave dispersion branch C^{-1} and C^{+1} is represented by the thin dotted lines and thin dash lines, respectively.

group velocities of lattice waves propagating in two opposite directions can be observed, which indicates the non-reciprocity.

4.2. Moderate autoparametric modulation

Then, we consider the moderate autoparametric modulation by setting $\Omega = 0.6124$. The numerical dispersion contours constructed from the response of the finite autoparametric super cell are evaluated with the parameters $\alpha = 0.75$, $\beta = [0.0167, 0.0833, 0.3333]$, $\gamma = 0.1667$, $\mu = 4$, $\theta = 0.5236$, and the amplitude $B_{0n} = 0.5\pi$. Remarkably, for the autoparametric structure, dynamic modulation

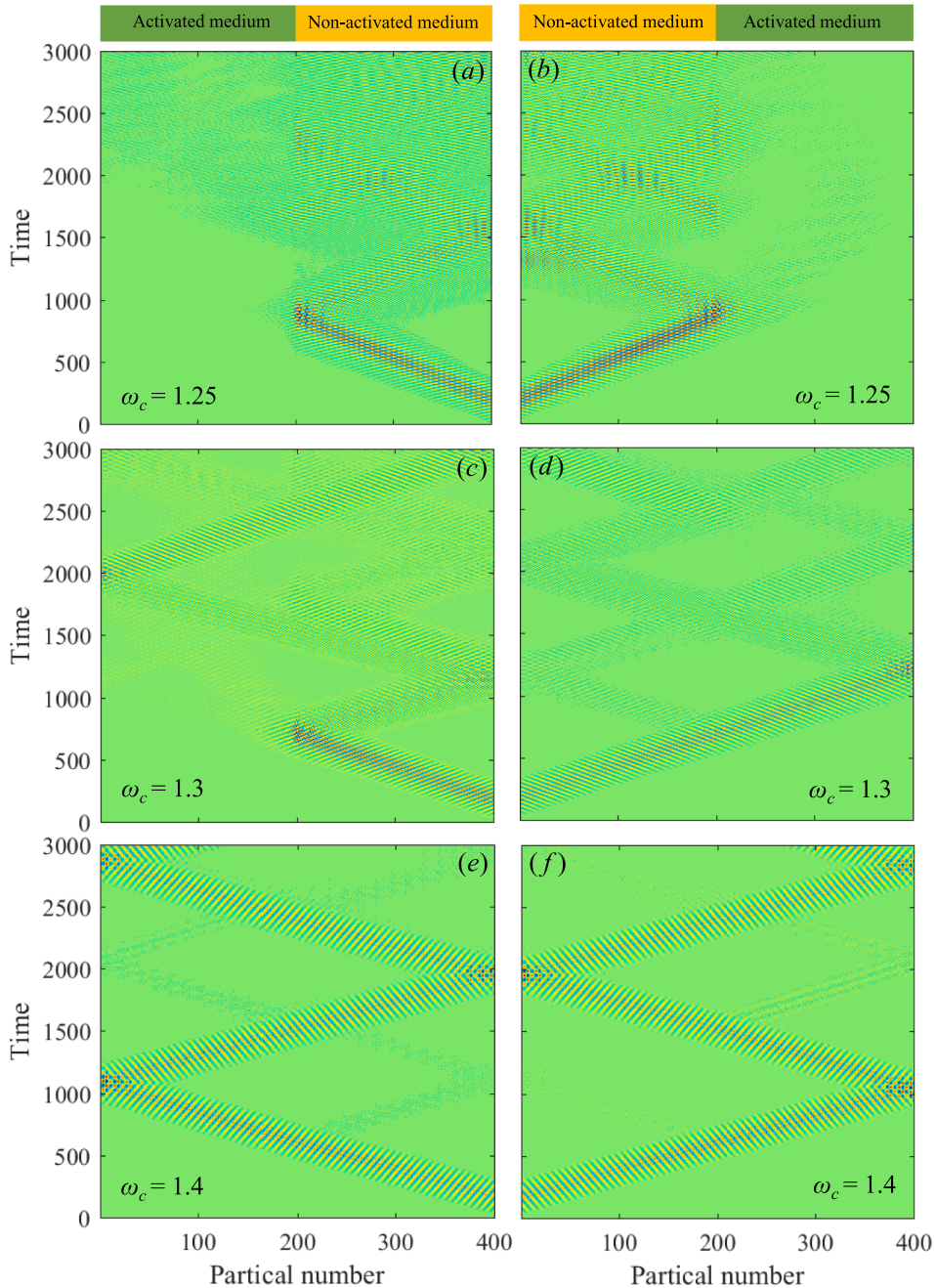


Fig. 6. (a, b) Spatiotemporal trajectory of partial displacement when signal is sent from the right and left end, respectively, with central frequency $\omega_c = 1.25$. (c, d) Spatiotemporal trajectory of partial displacement when signal is sent from the right and left end, respectively, with central frequency $\omega_c = 1.3$. (e, f) Spatiotemporal trajectory of partial displacement when signal is sent from the right and left end, respectively, with central frequency $\omega_c = 1.4$.

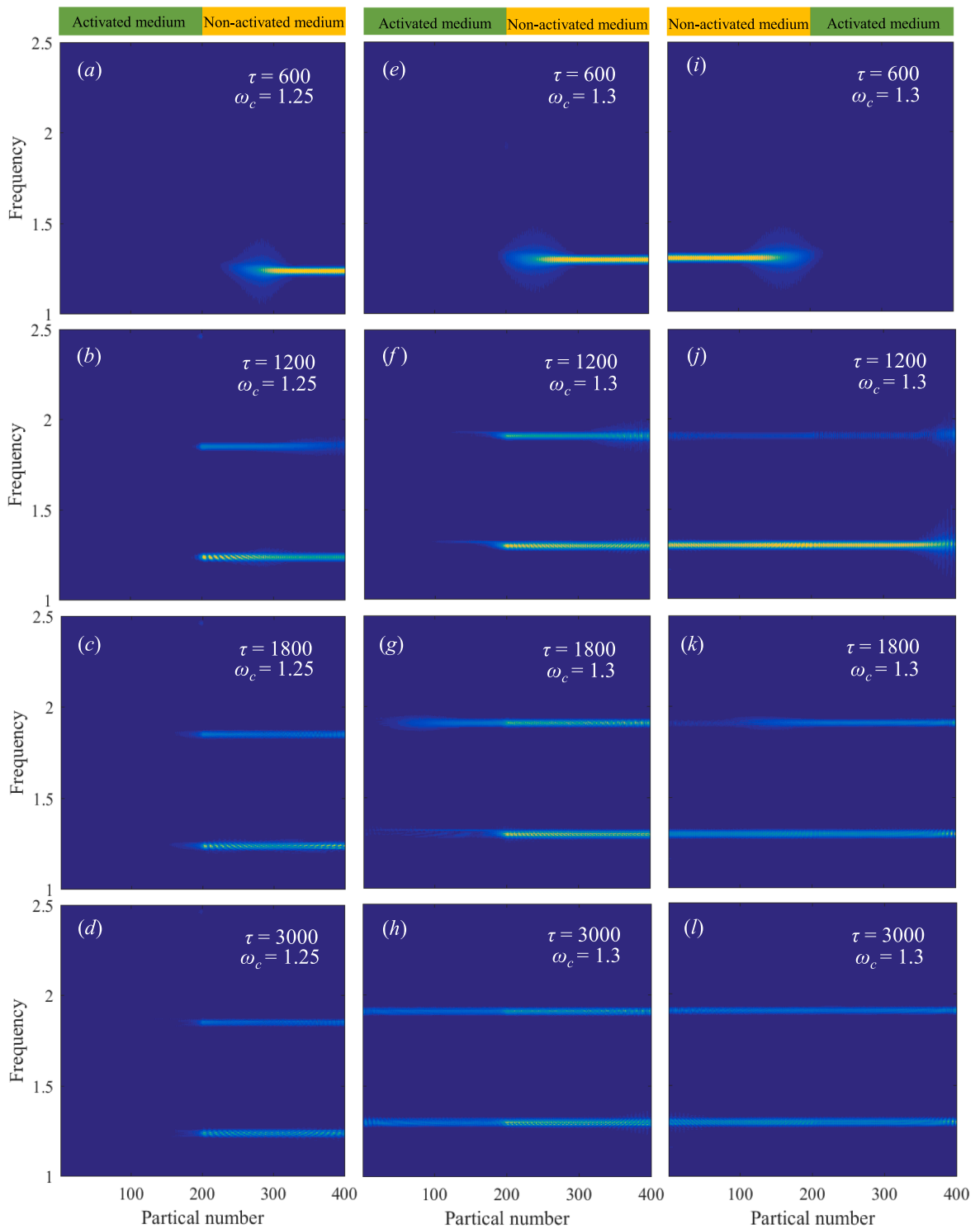


Fig. 7. The frequency content of the propagating pulse at the time 600, 1200, 1800 and 3000, respectively. (a-d) Signal is sent from the right with central frequency $\omega_c = 1.25$. (e-h) Signal is sent from the right with central frequency $\omega_c = 1.3$. (i-l) Signal is sent from the left with central frequency $\omega_c = 1.3$.

originates primarily from the fundamental mode of the chiral rotational DOF, and its frequency is related to both the global location of the band diagram in frequency domain and the strength of the autoparametric modulation as referred by Eq. (1). Based on the coupled mode theory, the incident wave dispersion branch C^0 represented by the thin solid lines (corresponding to the unmodulated case), and the scattered wave dispersion branch C^{-1} and C^{+1} represented by the thin dotted lines and thin dash lines, respectively, are separated and shown in Fig. 5. We make the important observation that there are four pairs of intersecting points of Bloch solutions (C^0 and $C^{\pm 1}$) in which asymmetric bandgaps generate. The loss of parity indicates that, if one wave is scattered when incident in a specific direction, it will be scattered or not when incident in the opposite direction, depending on the excitation frequency. We compare the band diagram obtained using full numerical simulations in the form of contour lines, with the band diagram that are given by the method of multiple-time scales with second-order accuracy as displayed in Fig. 5. The results show the good agreement between the numerical method and the analytical prediction proposed in this paper, even when the autoparametric modulation is relatively strong.

To verify the frequency-dependent wave non-reciprocity, we consider a composite structure made of autoparametric lattices with and without initially activated chiral rotational vibration. Short pulses with different central frequencies are sent from the right or left ends of a finite composite structure, and the wave responses are illustrated in Fig. 6. Fig. 6 (a) shows that, when the narrow-band displacement excitation with central frequency $\omega_c = 1.25$ is imposed at the right end of the non-activated medium side, the pulse wave is totally reflected with up-converted frequency upon impinging the activated/non-activated medium interface. The frequency difference induced by the autoparametric modulation is approximately equal to Ω , as evidenced by the spectrum contour of the propagating waves in Fig. 7 (a-d). The reflected waves propagating rightwards with two different frequencies and group velocities are reflected again at right ends without the change of wave frequencies and amplitudes. Since the incident frequency and up-converted frequency are within the forbidden band, multiple wave reflection occurs and is accompanied by the inter-flow of energy between the incident frequency and the up-converted frequency components. As the consequence of the multiple reflections, the pulse waves are constrained in the non-activated medium. The same wave propagation phenomenon can be observed in Fig. 6 (b) when the pulse is sent from the left end of the non-activated/activated medium.

The non-reciprocal wave propagation arises when the narrow-band displacement excitation with central frequency $\omega_c = 1.3$ is imposed at two ends of the composite mediums, as shown in Fig. 6 (c) and Fig. 6 (d). The corresponding frequency contours of propagating waves at different instants are illustrated in Fig. 7 (e-h) and Fig. 7 (i-l). For the activated/non-activated medium (Fig. 6 (c)), the pulse wave impinging the right end undergoes the reflection at the interface, and the activated autoparametric modulation induces a partial energy migration to the mode with higher frequency. After reflected again at the right end, these wave pulses with up-converted frequency propagate leftwards toward the interface. In contrast to the scenario in Fig. 6 (a), the up-converted frequency is now outside of the forbidden band. The left-travelling wave can penetrate the activated medium. At the left boundary of the activated medium, the waves are reflected with down-converted frequency such that a partial energy is migrated to the mode with the initial frequency ($\omega_c = 1.3$). This fundamental mode is outside the forbidden band and then can be transmitted into the non-activated autoparametric modulated medium.

For the non-activated/activated medium (Fig. 6 (d)), the pulse wave sent from the left end propagates across the interface with almost no reflection, and is transmitted into the activated medium. Then, it is reflected by the right boundary, accompanying by partial energy conversion into the mode with higher frequency. Since the up-converted frequency is outside of the forbidden band, the wave propagates leftwards into the non-activated medium, and is reflected back by the left boundary. When reaching the interface, the right-travelling wave is reflected and is accompanied by the inter-flow of energy between the incident frequency and the up-converted frequency components. We note that these frequency conversions can be readily realized if the incident wave frequency was set around the intersecting points of Bloch solutions, referring to Fig. 5. When the pulse central frequency $\omega_c = 1.4$ is set far from the intersecting points, reciprocal wave propagation can be observed as shown in Fig. 6 (e) and Fig. 6 (f).

4.3. Quasi-static autoparametric modulation

We finally analyze the autoparametric modulated structure in the quasi-static modulation. In this case, the rotational vibration frequency Ω in the autoparametric dynamical system is significantly small. Revisiting the perturbation procedure and substituting (25) into (4a), we have

$$\ddot{\mathbf{U}} + \mathbf{K}\mathbf{U} + \varepsilon\mathbf{N}\mathbf{L}_3 = \mathbf{0} \tag{27}$$

where

$$\mathbf{N}\mathbf{L}_3 = \begin{bmatrix} \chi_2 u_{3j} B_{01} \cos(\Omega\tau + \phi_1) \\ \chi_2 u_{3j+1} B_{02} \cos(\Omega\tau + \phi_2) \\ \chi_2 u_{3j+2} B_{03} \cos(\Omega\tau + \phi_3) \end{bmatrix} \tag{28}$$

It is noted that, since the slow modulation has been assumed, therefore, topological invariant based on the adiabatic theorem [25,26] can be adopted to investigate the band topology. Considering the dynamical system (27) with quasi-static stiffness evolution, the natural modes can then be directly obtained from the dynamic matrix at any instant.

Letting (ω_n^2, Ψ_n) be the instantaneous eigenvalue and eigenmode, defined by

$$(\mathbf{K}_\varepsilon - \omega_n^2 \mathbf{I}) \Psi_n = \mathbf{0} \tag{29}$$

where

$$\mathbf{K}_\xi = \mathbf{K} + \varepsilon \chi_2 \begin{bmatrix} B_{01} \cos(\Omega \tau + \phi_1) & 0 & 0 \\ 0 & B_{02} \cos(\Omega \tau + \phi_2) & 0 \\ 0 & 0 & B_{03} \cos(\Omega \tau + \phi_3) \end{bmatrix} \quad (30)$$

In order to describe the change of each dispersion band due to the quasi-static modulation, wavenumber and time are chosen as two independent variables and the Chern number corresponding to each band is characterized as follows

$$\mathcal{C}_n = \frac{1}{2\pi} \int_{-\pi}^{\pi} \int_0^T \mathcal{B}_{cn} d\tau d\xi \quad (31)$$

where the Berry curvature can be defined by

$$\mathcal{B}_{cn} = 2 \text{Im} \sum_{m \neq n} \frac{\langle \Psi_n, \partial_\xi \mathbf{K}_\xi, \Psi_m \rangle \langle \Psi_m, \partial_\tau \mathbf{K}_\xi, \Psi_n \rangle}{(\omega_n^2 - \omega_m^2)^2} \quad (32)$$

Fig. 8 illustrates the dispersion evolution of a modulated super cell with respect to wavenumber and time, and the corresponding Chern number of each band is labeled. The parameters used are $\alpha = 0.5$, $\beta = [0.0167, 0.0833, 0.3333]$, $\gamma = 0.1667$, $\mu = 400$, $\theta = 0.5236$, $B_{0n} = \pi$ and $\Omega = 0.05$. It is well known that the bandgap topology is manipulated by the gap Chern number, which is the summation of the Chern numbers of all the bands below it. For the 3-periodic super cell with the initial phase modulation $\phi_n = 2\pi n/3$ of its n -th sublattice, gap Chern numbers 0, -1, 1, 0 are associated with four bandgaps 1, 2, 3 and 4, respectively. Non-zero gap Chern numbers support the existence of topological edge states according to the principle of bulk-edge correspondence. We perform numerical simulations to show how eigenfrequencies of a finite super cell evolve over time as a result of the quasi-static wave-like modulation induced by the chiral vibration. It can be seen in Fig. 9 (a) that there are two pairs of edge modes populated within two bulk bandgaps, respectively, and the two non-zero gap Chern numbers indicate non-trivial band topology for the autoparametric system under quasi-static modulation and opposite signs of the Chern numbers associated with bandgaps 2 and 3 imply the opposite phase reversal related to the edge modes. To confirm the bulk-edge correspondence, we focus on the time evolution of eigenfrequencies inside the second bandgap and the corresponding eigenmodes along the finite super cell. The right edge mode labeled b (Fig. 9 (b)) is picked up as a starting point of the evolution flow. This edge mode evolves towards the bulk mode d (Fig. 9 (d)) via the right edge mode c (Fig. 9 (c)), accompanied by decreased frequency across the bandgap. As the frequency shifts up, bulk mode d (Fig. 9 (d)) transforms into the left edge mode e (Fig. 9 (e)), which then evolves towards the bulk mode g (Fig. 9 (g)) via the left edge mode f (Fig. 9 (f)). Then, bulk mode g evolves back into the right edge mode b and so on. For spatially modulated lattices, the topological pumping occurs at single frequency along the wave number branch of the edge state, and a complete right-to-left (or left-to-right) mode transition can be observed during one modulated cycle [42]. However, only transition between localized edge mode (right or left) and bulk mode can be seen for time-modulated lattices under the transient propagation of a physical signal in each cycle. It is evident that the absolute value of gap Chern number -1 for the second bandgap equals the number of degenerate points during one modulated cycle, actually also the number of times the right (or left) edge state traverses the bandgap. As a matter of fact, this kind of edge mode and mode transition can be employed to realize non-reciprocal transmission of the elastic waves [23]. Specifically, by exciting the system with right (left) edge state from the right (left) end of finite lattices at a certain time point, the longitudinal wave can propagate only from the right (left) to the left (right) end via the bulk state, due to the fact that the intrinsic mode of the lattices is triggered. However, the propagating wave

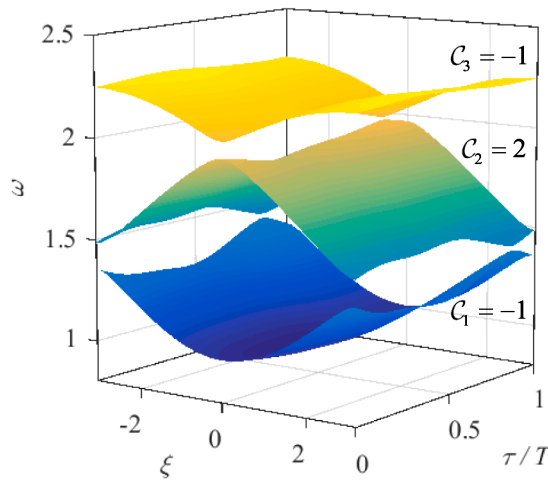


Fig. 8. Evolution of Bloch dispersion branches of an infinite periodic super cell as a function of wavenumber and time, with Chern numbers assigned to each band.

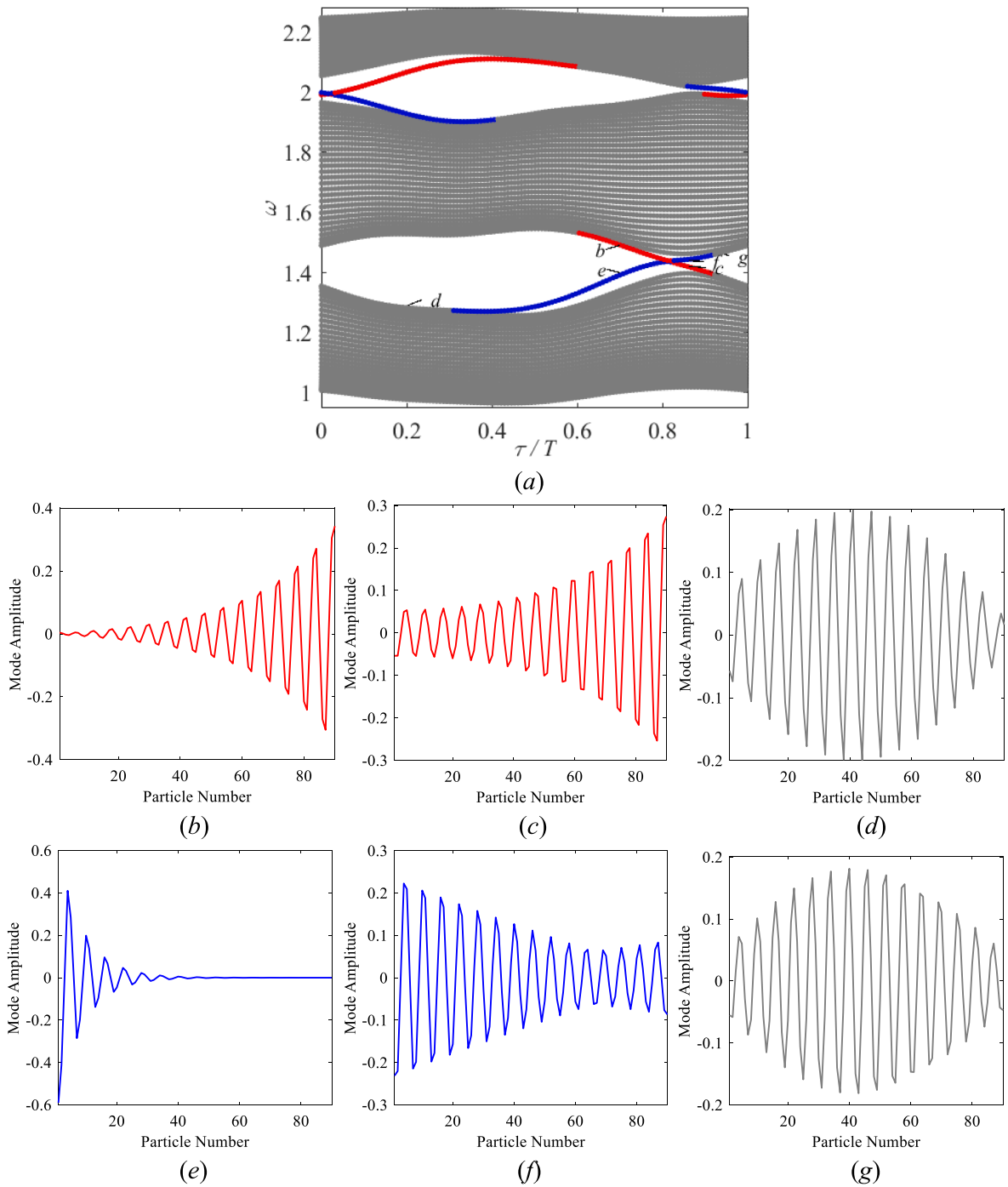


Fig. 9. (a) Evolution of eigenfrequencies of a finite periodic super cell over one period of slow modulation. The bulk modes are denoted by gray dots. Right and left edge modes are highlighted by red and blue and dots, respectively. The edge modes within the second bandgap at $\tau = 0.7 T$ and $\tau = 0.85 T$ are labeled *b*, *e*, and *c*, *f*; The bulk modes at $\tau = 0.2 T$ and $\tau = 0.95 T$ are labeled *d* and *g*. (b)-(g) The corresponding eigenmodes along the finite super cell. (For interpretation of the references to colour in this figure legend, the reader is referred to the web version of this article.)

from the left (right) to the right (left) is strictly forbidden if the excitation is imposed in the reverse direction, resulting from null energy input into the system at all (the intrinsic mode is not triggered). Moreover, the robustness of the topologically protected edge mode against dissipation effects and modulation phase disorders can also be rationally expected [26].

5. Conclusion

In this paper, a novel class of nonlinear chiral-induced autoparametric periodic structure is proposed. By combining multiple-time scales perturbation method and Floquet-Bloch theorem, a procedure for analytically deriving the evolution equations and solving the dispersion relations of autoparametric systems is presented. Numerical simulations are performed to validate the global dynamics, the analytical band diagram and demonstrate the non-reciprocal wave propagation on the dynamically modulated system. The band topology of wave dispersion and bulk edge correspondence in the quasi-static scenario are also investigated.

It is remarkable that the proposed autoparametric modulated structure could be designed as functional devices possessing outstanding direction-dependent propagation properties and the analytical approach with second-order accuracy can capture the asymmetry of dispersion curves in the case of relatively strong nonlinearity. In the sense of small-on-large, the autoparametric modulated structure is degenerated into a spatiotemporally modulated periodic structure, which is an ideal platform to implement a mechanical analogue of the quantum Hall effect in a periodic super cell under quasi-static modulation. The proposed autoparametric modulated concept based on geometric nonlinearity for tailoring the wave propagation could be used to construct various 2D and 3D composite structures with exotic wave manipulation capacity in passive or active ways.

CRedit authorship contribution statement

Tianjun Yu: Conceptualization, Investigation, Visualization, Writing – original draft. **Yong Cheng:** Visualization, Writing – original draft. **Sha Zhou:** Methodology, Supervision, Validation, Writing – review & editing.

Declaration of Competing Interest

The authors declare that they have no known competing financial interests or personal relationships that could have appeared to influence the work reported in this paper.

Acknowledgements

The authors gratefully acknowledge the financial support from the National Natural Science Foundation of China under Grant No. 11802016 and 11802266, the National Key R&D Program of China (2018YFC0809400) and the China Postdoctoral Science Foundation (2018M631349). The authors wish to thank Professor X.M. Zhou for fruitful discussions.

References

- [1] R. Fleury, D.L. Sounas, C.F. Sieck, M.R. Haberman, A. Alù, Sound isolation and giant linear nonreciprocity in compact acoustic circulator, *Science* 343 (2014) 516–519.
- [2] H. Nassar, B. Yousefzadeh, R. Fleury, M. Ruzzene, A. Alù, C. Daraio, A.N. Norris, G. Huang, M.R. Haberman, Nonreciprocity in acoustic and elastic materials, *Nat. Rev. Mater.* 5 (9) (2020) 667–685.
- [3] L.M. Nash, D. Kleckner, A. Read, V. Vitelli, A.M. Turner, W.T.M. Irvine, Topological mechanics of gyroscopic metamaterials, *Proc. Natl. Acad. Sci. U. S. A.* 112 (47) (2015) 14495–14500.
- [4] P. Wang, L. Lu, K. Bertoldi, Topological phononic crystals with one-way elastic edge waves, *Phys. Rev. Lett.* 115 (2015), 104302.
- [5] B. Liang, X.S. Guo, J. Tu, D. Zhang, J.C. Cheng, An acoustic rectifier, *Nat. Mater.* 9 (12) (2010) 989–992.
- [6] N. Boechler, G. Theoharis, C. Daraio, Bifurcation-based acoustic switching and rectification, *Nat. Mater.* 10 (9) (2011) 665–668.
- [7] C. Liu, Z.L. Du, Z. Sun, H.J. Gao, X. Guo, Frequency-preserved acoustic diode model with high forward-power-transmission rate, *Phys. Rev. Appl.* 3 (2015), 064014.
- [8] C.Y. Fu, B.H. Wang, T.F. Zhao, C.Q. Chen, High efficiency and broadband acoustic diodes, *Appl. Phys. Lett.* 112 (2018), 051902.
- [9] Z.-N. Li, Y.-Z. Wang, Y.-S. Wang, Nonreciprocal phenomenon in nonlinear elastic wave metamaterials with continuous properties, *Int. J. Solids Struct.* 150 (2018) 125–134.
- [10] Z.N. Li, Y.Z. Wang, Y.S. Wang, Tunable nonreciprocal transmission in nonlinear elastic wave metamaterials by initial stresses, *Int. J. Solids Struct.* 182 (2020) 218–235.
- [11] L.S. Lin, Y.Z. Wang, Y.S. Wang, Nonreciprocal transmission of nonlinear elastic wave metamaterials by incremental harmonic balance method, *Int. J. Mech. Sci.* 173 (2020), 105433.
- [12] N. Swintek, S. Matsuo, K. Runge, J.O. Vasseur, P. Lucas, P.A. Deymier, Bulk elastic waves with unidirectional backscattering-immune topological states in a time-dependent superlattice, *J. Appl. Phys.* 118 (2015), 063103.
- [13] G. Trainiti, M. Ruzzene, Non-reciprocal elastic wave propagation in spatiotemporal periodic structures, *New J. Phys.* 18 (2016), 083047.
- [14] J. Vila, R.K. Pal, M. Ruzzene, G. Trainiti, A Bloch-based procedure for dispersion analysis of lattices with periodic time-varying properties, *J. Sound Vib.* 406 (2017) 363–377.
- [15] H. Nassar, H. Chen, A.N. Norris, M.R. Haberman, G.L. Huang, Non-reciprocal wave propagation in modulated elastic metamaterials, *Proc. R. Soc. A* 473 (2017) 20170188.
- [16] H. Nassar, X.C. Xu, A.N. Norris, G.L. Huang, Modulated phononic crystals: non-reciprocal wave propagation and Willis materials, *J. Mech. Phys. Solids* 101 (2017) 10–29.
- [17] K. Yi, S. Karkar, M. Collet, One-way energy insulation using time-space modulated structures, *J. Sound Vib.* 429 (2018) 162–175.
- [18] J. Huang, X. Zhou, A time-varying mass metamaterial for non-reciprocal wave propagation, *Int. J. Solids Struct.* 164 (2019) 25–36.
- [19] J.H. Huang, X.M. Zhou, Non-reciprocal metamaterials with simultaneously time-varying stiffness and mass, *ASME J. Appl. Mech.* 87 (2020), 071003.
- [20] A. Palermo, P. Celli, B. Yousefzadeh, C. Daraio, A. Marzani, Surface wave non-reciprocity via time-modulated metamaterials, *J. Mech. Phys. Solids* 145 (2020), 104181.
- [21] Y.F. Wang, B. Yousefzadeh, H. Chen, H. Nassar, G.L. Huang, C. Daraio, Observation of nonreciprocal wave propagation in a dynamic phononic lattice, *Phys. Rev. Lett.* 121 (2018), 194301.
- [22] M.A. Attarzadeh, J. Callanan, M. Nouh, Experimental observation of nonreciprocal waves in a resonant metamaterial beam, *Phys. Rev. Appl.* 13 (2) (2020), <https://doi.org/10.1103/PhysRevApplied.13.021001>.

- [23] R. Chaunsali, F. Li, J.K. Yang, Stress wave isolation by purely mechanical topological phononic crystals, *Sci. Rep.-UK* 6 (2016) 30662.
- [24] S.P. Wallen, M.R. Haberman, Nonreciprocal wave phenomena in spring-mass chains with effective stiffness modulation induced by geometric nonlinearity, *Phys. Rev. E* 99 (2019), 013001.
- [25] H. Nassar, H. Chen, A.N. Norris, G.L. Huang, Quantization of band tilting in modulated phononic crystals, *Phys. Rev. B* 97 (2018), 014305.
- [26] H. Chen, L.Y. Yao, H. Nassar, G.L. Huang, Mechanical quantum Hall effect in time-modulated elastic materials, *Phys. Rev. Appl.* 11 (2019), 044029.
- [27] A. Tondl, T. Ruijgrok, F. Verhulst, R. Nabergoj, *Autoparametric Resonance in Mechanical Systems*, Cambridge University Press, 2000.
- [28] T.J. Yu, W. Zhang, X.D. Yang, Global dynamics of an autoparametric beam structure, *Nonlinear Dyn.* 88 (2) (2017) 1329–1343.
- [29] Z.Y. Liu, X.X. Zhang, Y.W. Mao, Y.Y. Zhu, Z. Yang, C.T. Chan, P. Sheng, Locally resonant sonic materials, *Science* 289 (2000) 1734–1736.
- [30] N. Fang, D. Xi, J. Xu, M. Ambati, W. Srituravanich, C. Sun, X. Zhang, Ultrasonic metamaterials with negative modulus, *Nat. Mater.* 5 (6) (2006) 452–456.
- [31] X.N. Liu, G.K. Hu, G.L. Huang, C.T. Sun, An elastic metamaterial with simultaneously negative mass density and bulk modulus, *Appl. Phys. Lett.* 98 (2011), 251907.
- [32] R. Zhu, X.N. Liu, G.K. Hu, C.T. Sun, G.L. Huang, Negative refraction of elastic waves at the deep subwavelength scale in a single-phase metamaterial, *Nat. Commun.* 5 (2014) 5510.
- [33] G.B. Hu, A.C.M. Austin, V. Sorokin, L.H. Tang, Metamaterial beam with graded local resonators for broadband vibration suppression, *Mech. Syst. Signal Process.* 146 (2021), 106982.
- [34] T.J. Yu, S. Zhou, Power generation mechanism and performance analysis of parametrically excited piezoelectric composite devices for vibratory energy harvesting, *Compos. Struct.* 275 (2021) 114462.
- [35] M.A. Campana, M. Ouisse, E. Sadoulet-Reboul, M. Ruzzene, S. Neild, F. Scarpa, Impact of non-linear resonators in periodic structures using a perturbation approach, *Mech. Syst. Signal Process.* 135 (2020), 106408.
- [36] Yu T.J., Cheng Y., Zhou S., **Non-reciprocity and selective wave amplifying in nonlinear inertia-induced autoparametric periodic structures**, 2021.
- [37] R.K. Nariseti, M.J. Leamy, M. Ruzzene, A perturbation approach for predicting wave propagation in one-dimensional nonlinear periodic structures, *ASME J. Vib. Acoust.* 132 (2010), 031001.
- [38] T.J. Yu, W. Zhang, X.D. Yang, Nonlinear dynamics of flexible L-shaped beam based on exact modes truncation, *Int. J. Bifurcat. Chaos.* 27 (2017) 1750035.
- [39] M.D. Fronk, M.J. Leamy, M. Ruzzene, High-order dispersion, stability, and waveform invariance in nonlinear monoatomic and diatomic systems, *ASME J. Vib. Acoust.* 139 (2017), 051003.
- [40] A.H. Nayfeh, D.T. Mook, *Nonlinear Oscillations*, Wiley, 1995.
- [41] S.S. Yao, X.M. Zhou, G.K. Hu, Investigation of the negative-mass behaviors occurring below a cut-off frequency, *New J. Phys.* 12 (2010), 103025.
- [42] M.I.N. Rosa, R.K. Pal, J.R.F. Arruda, M. Ruzzene, Edge states and topological pumping in spatially modulated elastic lattices, *Phys. Rev. Lett.* 123 (2019), 034301.